Aloke Kumar
School of Mechanical Engineering,
and Birck Nanotechnology Center,
Purdue University,
West Lafayette, IN 47907

Venu M. Gorti[1]
School of Mechanical Engineering,
Purdue University,
West Lafayette, IN 47907

Hao Shang[2]
School of Chemical and Biomedical Engineering,
Purdue University,
West Lafayette, IN 47907

Gil U. Lee
School of Chemical and Biomedical Engineering,
and Birck Nanotechnology Center,
Purdue University,
West Lafayette, IN 47907

Nung Kwan Yip
Department of Mathematics,
Purdue University,
West Lafayette, IN 47907

Steve T. Wereley[3]
School of Mechanical Engineering,
and Birck Nanotechnology Center,
Purdue University,
West Lafayette, IN 47907
e-mail: wereley@purdue.edu

Optical Diffusometry Techniques and Applications in Biological Agent Detection

Optical diffusometry is a technique used for measuring diffusion. This work explores the possibility of directly measuring diffusion coefficients of submicron particles for pathogen detection. The diffusion coefficient of these particles is a function of the drag coefficient of the particle at constant temperatures. Particles introduced into a sample containing an analyte bind with the analyte if functionalized with the appropriate antibodies. This leads to an increase in the hydrodynamic drag of the particles and hence a decrease in their diffusion coefficient. This study uses the above principle to effectively measure the diffusion coefficient of the particles using two different experimental approaches. The measured reduction in the diffusion coefficient can be correlated to the amount of analyte present and thus forms the basis of biological agent detection. Sensitivity to experimental conditions is analyzed. It is observed that alternative techniques such as optical trapping hold promise: the diffusive behavior of particles in optical traps is found to be quantitatively different from that of a free particle. Hence preconditions are identified to make optical trapping appropriate for agent detection. [DOI: 10.1115/1.2969430]

Introduction

The early work of Einstein [1], Smoluchowski [2], and Langevin [3] established the much needed theoretical framework required to understand Brownian motion. The strange jiggling motion of the pollen grains was first documented by Brown, but it took an intuitive leap when Einstein [1] explained the underlying physical mechanism behind the phenomenon. Based on the molecular kinetic theory of heat and the fluctuation-dissipation theorem, Einstein deduced that the diffusion coefficient (D) of the particle is related to the viscous frictional resistance (ξ) in the following form:

$$D = \frac{kT}{\xi} \tag{1}$$

where k is the Boltzmann constant and T is the temperature. See also Ref. [4] for a contemporary treatment.

For spherical particles with radius r and low Reynolds number flow, ξ is well approximated by Stokes' law [5],

$$\xi = 6\pi\mu r \tag{2}$$

where μ is the viscosity of water.

From the above formula, the diffusion coefficient of submicron particles can be used to measure the temperature of the fluid at small length scales, the local fluid viscosity, and also the particle size. Recently, several researchers [6–9] studied the Brownian motion of submicron sized particles suspended in a fluid using digital video microscopy. Crocker [6] made use of optical traps to study the hydrodynamic correction to Brownian motion for the case of two spheres in close proximity. They demonstrated with carefully designed experiments that the diffusion coefficient can be experimentally measured to an accuracy of $\pm 1\%$. Nakroshis et al. [10] measured the Boltzmann constant, whereas Salmon et al. [9] measured Avogadro's number by studying the Brownian motion of submicron sized particles.

The present work explores the process of measuring the mean diffusion coefficient of a population of nearly identical virus-tagged rigid spherical particles. It is motivated by the idea that the binding of viruses on antibody functionalized particles should result in a measurable change in the diffusion coefficient. Such a decrease can be measured by the observation of particles, which are freely moving or are held in a region by an optical trap. Thus the objective is to establish optical diffusometry as a viable technique for biosensing, which is the name given to a host of technologies designed to detect the presence of biological analytes in a solution. These technologies use recognition elements such as antibodies, DNA, receptor proteins, and biomimetic elements for the above stated purpose. These methods include, but are not limited to, immunoassays [11], enzyme-catalyzed reactions [12], surface plasmon resonance technique [13], and impedimetric methods [14,15]. Optical methods for biosensing were explored by Anderson et al. [11] who developed a portable and automated

[1]Present address: Hindustan Unilever Limited, Mumbai, India.
[2]Present address: MagSense Life Sciences Inc., USA.
[3]Corresponding author.

Contributed by the Fluids Engineering Division of ASME for publication in the JOURNAL OF FLUIDS ENGINEERING. Manuscript received June 22, 2007; final manuscript received June 11, 2008; published online September 22, 2008. Assoc. Editor: Juergen Kompenhans.

optical biosensor called RAPTOR to perform immunoassays. Fluorescence intensity was used to quantify the presence of antigens in a sample. Cui et al. [16] showed that binding of an analyte to the surface of a silicon nanowire leads to an observable change in the electrical conductivity of a medium. Such methods provide a basis for sensitive sensors to detect chemical and biological species. Typically, affinity biosensors use sandwich assays for detection and measurement. One drawback of sandwich assays is the difficulty in producing two antibodies that each bind to different sites of an antigen. Also, the probability of two binding events on a single antigen is less than that of a single binding event.

Most of the prevalent biological agent detection methods suffer from the disadvantage of being an indirect method. The present work explores different optical diffusometry techniques and establishes these as direct means of pathogen detection. The principles underlying all of them are discussed in detail, and the advantages and disadvantages of each are examined.

Experimental Techniques for Optical Diffusometry

This section discusses two experimental techniques—particle tracking and micron resolution particle image velocimetry (μPIV).

Particle Tracking. Einstein, in his pioneering work [1], defined the diffusion coefficient in terms of a measurable property of Brownian motion—the mean square displacement of particles. These quantities are related by

$$\langle \Delta x^2 \rangle = 2nD\Delta t \tag{3}$$

where Δx is the displacement of the Brownian particle over a period of time Δt, the brackets $\langle \cdot \rangle$ refer to the statistical average of the contained quantity, and n is the number of degrees of translational freedom.

In particle tracking the motion of individual particles as a function of time is measured, and then Eq. (3) is applied to find the diffusion coefficient [7,17]. The accuracy and practicability of using diffusometry as a means of biological agent detection strongly depends on how the mean square displacement $\langle \Delta x^2 \rangle$ is determined. For this a discrete approach to position detection is undertaken by analyzing a sequence of images.

Particle position detection requires a position acquisition system, usually a video microscopy system. The particles undergoing Brownian motion are imaged at a fixed time interval using a video camera or a charge coupled device (CCD) camera attached to a microscope. Particle tracking can be done for a single or for multiple particles. The former, as the name suggests, involves tracking a single particle. The more advanced multiple particle tracking method tracks multiple particles simultaneously and recovers track data for each particle.

An accurate calculation of diffusion coefficient relies directly on the ability to track and identify particles. Einstein's original formulation assumes negligible boundary effects on the random motion of particles. To achieve such a condition experimentally, the focal plane of objective lens was adjusted so that each imaged particle is several particle diameters away from the wall. The particles were imaged using fluorescence microscopy, and a CCD camera (CoolSnap HQ, Photometrics, Tuscon, AZ) was used to acquire images at specified intervals. The camera has a 1392 $\times$1040 element CCD at 6.45$\times$6.45 μm^2 pixel pitch. Image acquisition was controlled using the METAMORPH software package (Universal Imaging Corp., PA). The exposure time was set at 10 ms, and the time between images was 300 ms. The images were filtered using wavelet transformation to improve the signal-to-noise ratio. These images were then processed to yield the location of particle centers. Local maxima were first found with pixel level accuracy and the centers were located with subpixel accuracy using Gaussian curve fitting. Selecting only those maxima, which were above a certain threshold level, ensured that the particles being selected were in the vicinity of the focal plane of the objective lens.

The objective lens had a magnification of 20$\times$, and the resulting field of view had 10–20 particles per image. The center locations of the particles in the images were analyzed using a MATLAB® adaptation of the IDL particle tracking software developed by Grier, Crocker, and Weeks. The adaptation by Blair and Dufresne is freely available for public use [18].

Referring to Eq. (3), we see that the equation is statistical in nature and that the accuracy in the computation of diffusion coefficient is limited by the accuracy of the measured value of displacement values. Pixelation of data is the foremost source of error in the above discussed methodology. However, with Gaussian curve fitting, an accuracy of a tenth of a pixel can be achieved for particles of this size. The accuracy of subpixel location is directly correlated to the original size of the object being located. It is simply a biasing of the brightest portion of the feature of interest, weighed by the location of neighboring bright areas. In addition Eq. (3) ideally requires an infinite sample size, but this is clearly not possible. In accordance with statistical theory, the error reduces with an increase in sample size. Hence care should be taken to ensure that an adequate number of images are processed in order to arrive at an accurate value of the diffusion coefficient.

μ-PIV. μ-PIV uses instantaneous and ensemble-averaged flow fields in micron-scale fluidic devices. μ-PIV is now an established nonintrusive technique to obtain accurate velocity data with high spatial resolution and is widely used as a design tool for microfluidic devices. Like the setup of Santiago et al. [19], epifluorescent microscopy with micron sized ($\sim$700 nm) seed particles was used, and a CCD camera was used to record high-resolution particle-image fields. Although μ-PIV is primarily used to measure velocity fields, for small seed particles ($<$1 μm) and low speed flow ($<$10 μm/s), information regarding temperature and Brownian motion behavior can be extracted from the flow field. The basis for such extraction was laid out by the work of Olsen and Adrian [20] who showed that at such small scales errors from Brownian motion were significant enough to contribute to errors in the μ-PIV velocity measurements. It was later shown [21] that the broadening of the signal peak in the cross-correlation function is the key to measuring temperature using PIV. Olsen and Adrian [20], using theoretical considerations, derived equations describing the shape and height of the cross-correlation function in the presence of Brownian motion for both light-sheet illumination and volume illumination, which is used in μ-PIV. A minor manipulation of those equations (Eqs. (11) and (12) of Ref. [21]) shows that the diffusion coefficient can be related to the signal width by

$$2D\Delta t = \frac{\Delta s_{o,c}^2 - \Delta s_{o,a}^2}{8M^2} \tag{4}$$

where $\Delta s_{o,c}^2$ is the width of the correlation peak with Brownian motion, $\Delta s_{o,a}^2$ is the width of the correlation peak without Brownian motion, and M is the magnification of the objective lens. It should be noted that in any experiment, even where Brownian motion is significant, a computation of the autocorrelation function of one of the PIV image pairs yields $\Delta s_{o,a}^2$.

Assessment of Optical Traps for Diffusometry Measurements

Both the previous methods use a population of particles. Biosensing, based on diffusion differential, can be made more precise if such a differential could be established for single particles. Such a method can even allow for the identification of a single virus-tagged particle in a population of bare particles. A proposed solution is to trap a bead and hence confine them to a given spatial domain. Such a technique enables also the acquisition of a large amount of data in a single experiment. On the other hand, the

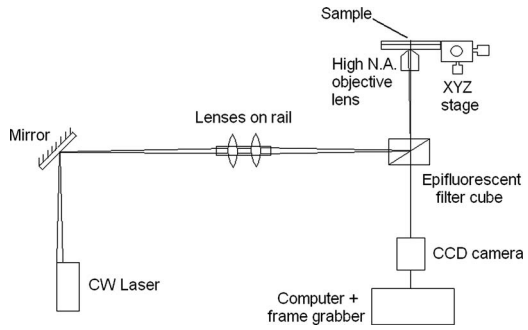

Fig. 1 Experimental setup for optical trapping. The lenses on the rail expand the beam, while the objective lens focuses the beam onto a diffraction limited spot. Epifluorescent imaging enhances the image quality.

aforementioned two methods suffer from the disadvantage that particles often escape out of the field of view, thus leading to loss of efficiency and also to errors.

Optical trapping appeared as a revolutionary technique for manipulating microscale particles around 1970 in a series of path-breaking experiments conducted by Ashkin in Bell Laboratories [22]. Although Ashkin originally used both single and dual light beams to guide and confine particles, the former soon grew in popularity and is now commonly referred to by the name "optical tweezers." Since their invention, optical tweezers have proven themselves to be a very powerful interdisciplinary tool. For instance, they have found extensive use in biophysics, as they serve as unique tools to manipulate and study single molecules of DNA [22–24]. Optically trapped beads have been successfully utilized to study cellular mechanics and structures [25,26]. Ashkin [27] provided an overview of the diverse uses of optical traps as a significant tool in various important areas of research.

Figure 1 shows the setup for the optical tweezers. Like other typical designs, it uses a laser beam that is suitably expanded, shaped, and focused through a high numerical aperture (NA) microscope objective lens. The laser has a TEM_{00} (transverse electric magnetic) mode, which eliminates inefficiency due to excessive laser modes. The laser beam is focused by an optical train to a diffraction limited spot where stable three dimensional trapping can be achieved. The size of the diffraction limited spot is mainly a function of the wavelength of trapping light used and the NA of the objective lens used [28]. The optical path consists of lenses, directing mirrors, and a filter cube, which is set up to specifically enable fluorescent imaging. The various practical and theoretical aspects involved in setting up a laser trap are discussed by Smith et al. [28] and Bechhoefer and Wilson [29]. The sample is held on an *XYZ* translational stage that serves primarily to focus the sample and also to laterally displace the sample. The functionalized microparticles are basically dielectric particles with submicron dimensions, hence in an intermediate range between Rayleigh and geometric optics regimes. The forces from the optical trap in this case arise from (i) the scattering (or radiative) force originated by momentum changes of light due to scattering and (ii) the gradient (or dipole) force caused by the Lorentz force acting on the induced dipole [22,27]. The scattering force is proportional to the laser intensity, and its effect is to push the particle along the axis of laser beam propagation while the gradient force moves the particle along the gradient of the optical field. An optical trap for the purpose of the present work can be considered to be akin to a potential well with a constant stiffness. Such characterization of a trap is useful for both the Rayleigh and Mie regimes [30,31]. Diffusion measurements for particles in a trap were done using an IEEE 1394 digital camera (Foculus, NET USA, Inc.).

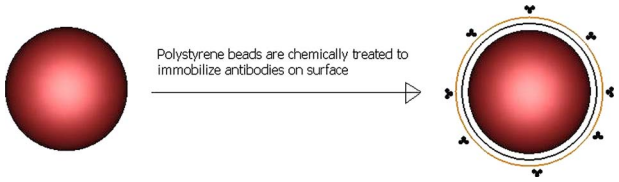

Fig. 2 Polystyrene beads are made to undergo a series of chemical processes so that a monolayer of poly(ethylene glycol) (PEG) is formed, and subsequently antibodies are immobilized on the PEG monolayer. The viruses bind onto the antibodies, thus leading to functionalized particles.

Optical Diffusometry and Biological Agent Detection

As indicated earlier, pathogen detection is achieved by virus tagging bare polystyrene beads. Such tagging is achieved by first coating the bead with appropriate antibodies (Fig. 2). These antibodies contain functional groups, which allow them to bind with certain proteins on the surface of the bead and hence make binding possible. In this work the M13 phage virus was used, and antibodies against the pVIII surface protein of the M13 phage virus were used. The M13 phage virus is filamentous in nature, with an approximate diameter of 6.5 nm and a length of 930 nm [32]. The detailed chemistry of functionalization of beads has been provided elsewhere [33].

Green fluorescent microspheres (diameter of 0.71 μm, excitation maximum of 468 nm, and emission maximum of 508 nm) and red fluorescent microspheres (diameter of 0.69 μm, excitation maximum of 542 nm, and emission maximum of 612 nm) were acquired from Duke Scientific Co. (Palo Alto, CA). Both types of particles were made of polystyrene latex, which has a density of 1.05 g/cm^3. The M13 phage was obtained from New England BioLabs Inc. (Beverly, MA), and the antibodies against the pVIII protein of the M13 phage were obtained from Pharmacia (Piscataway, NJ).

Results

The viability of the proposed technique was tested by incubating known concentrations of virus with known densities of particles and by subsequently measuring the change in the diffusion coefficient of the particles. The green particles were used in unmodified form, while the red ones were coated with an anti-pVIII antibody. The antibody-coated red beads were incubated with the M13 virus at ratios of 2:1, 6:1, 8:1, and 10:1 viruses per particle. At the end of the incubation reaction, the unmodified green particles were added to the solution of red particles. The diffusion coefficients of the mixture of antibody functionalized red particles and unmodified green particles were measured as a function of M13 concentration. This methodology was followed to ensure that both bead populations are subjected to identical external conditions.

As mentioned earlier the particles were imaged using fluorescence microscopy, which affords the user selective imaging of red or green particles by simply interchanging filter cubes. In Fig. 3(*a*) the particles in and near the focal plane are the ones sharpest in feature, and diffuse images represent particles considerably removed from the focal plane. Subsequently these images are filtered to improve the signal-to-noise ratio (Fig. 3(*b*)). From an ensemble of such images, the position values are processed to yield track information about individual particles. It should be pointed out that particles often leave the field of view or migrate away from the plane of focus, leading to loss of efficiency. Brownian motion is often stated as the random walk motion of small particles suspended in a fluid due to bombardment by molecules obeying a Maxwellian velocity distribution. The tracks appear to demonstrate the random walk behavior that the particles are expected to show (Fig. 4).

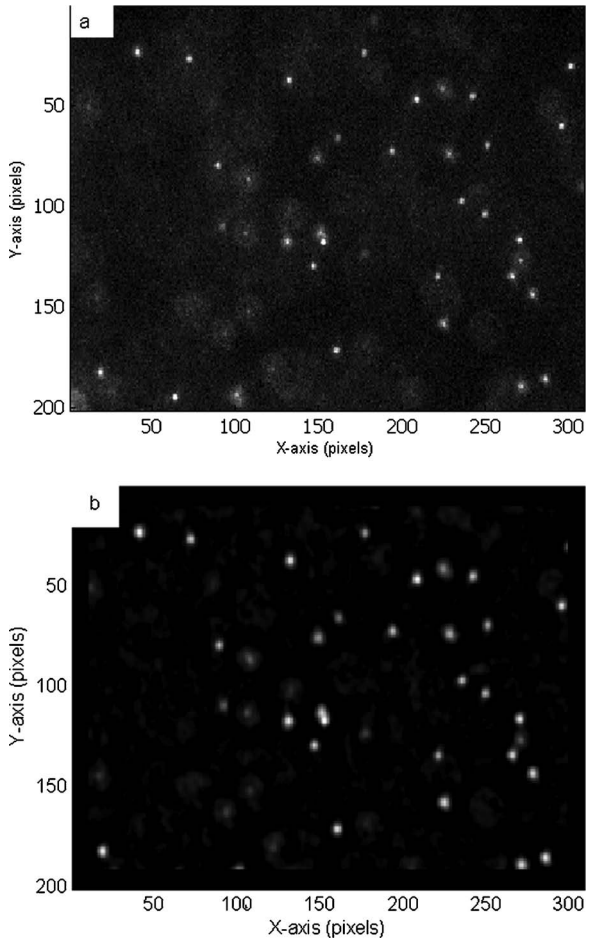

Fig. 3 Red microparticles (0.69 μm) functionalized with viruses are visualized using fluorescent microscopy. Note that fluorescent particles of only one type can be imaged at a time. (*a*) Fluorescent red particles can be seen as white dots on a black background. (*b*) The same image is filtered to enhance image quality. For particle tracking only, particles with intensity above a certain threshold are taken into account.

Figure 5 presents the diffusion coefficients measured for the particles without anti-pVIII antibodies and with antibodies in the

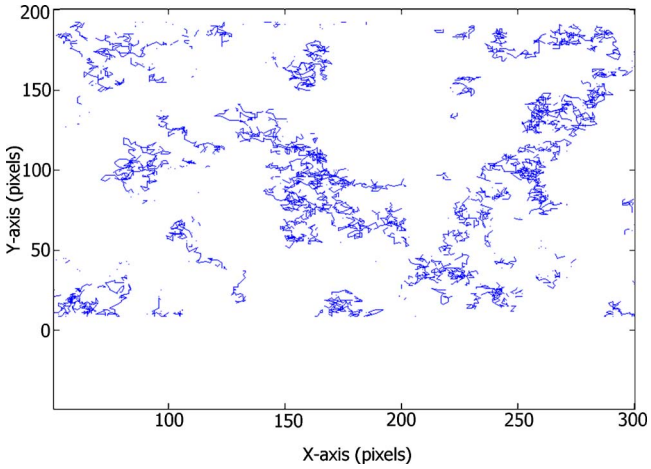

Fig. 4 A large number of images are processed to yield particle tracks. The terminated paths indicate loss of particle from the viewing volume.

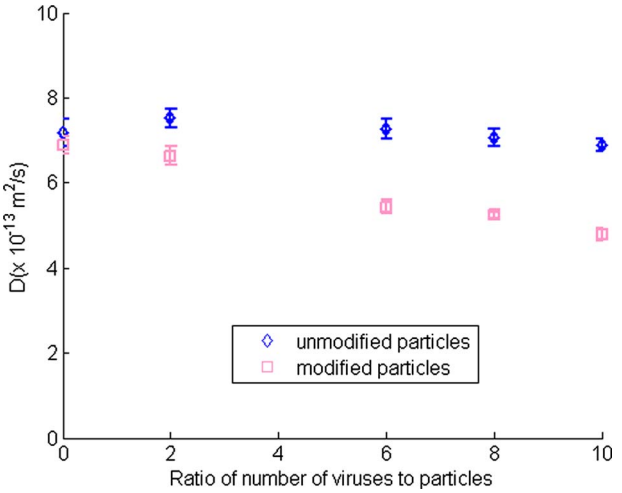

Fig. 5 Diffusion coefficients of antibody functionalized particles and unmodified particles as a function of virus concentration

presence of increasing virus concentrations. The significance of changes in the diffusion coefficients of the two populations was tested using analysis of variance (ANOVA). Both interpopulation and intrapopulation variances were tested, and it was found that for green particles, the variation in diffusion coefficient is not significant (p-value$=8.6\times10^{-8}$). However for red particles the variation in diffusion coefficient is found to be significant (p-value$=0.087$). The analysis indicates that virus tagging of red particles is the principal factor leading to a change in diffusion behavior. The diffusion coefficient values plotted here were obtained from a particle tracking analysis and were confirmed using μ-PIV.

A first order model for diffusion of 0.69 μm particles functionalized with antibodies and incubated with M13 viruses is constructed based on experimental findings. We assume in this simplified model that the virus tagging results in an increase in drag and that this increase is linear in nature. Specifically, the model assumes that the diffusion coefficient of tagged particles is given by

$$D = \frac{kT}{\xi_{\text{virus}} + \xi_{\text{sphere}}} \tag{5}$$

where ξ_{virus} increases linearly with an increase in virus concentration.

A least squares fit yields the following correlation

$$\xi_{\text{total}} = \xi_{\text{sphere}} + \xi_{\text{virus}} = (0.2705 n_{\text{virus}} + 5.863) \times 10^{-9} \text{ N s/m} \tag{6}$$

The variable n_{virus} represents viruses per particle and assumes a value from the set {2, 6, 8, 10}. The goodness of the fit is characterized by the R^2 value, and its high value of 0.98 for the above fit suggests the adequacy of the linear model.

One of the primary sources of systematic error that results from the use of images is pixelation. An estimate of error due to digitization (pixelation in the case of video microscopy) loss can be gauged from Fig. 6. The figure depicts experimental error in the calculation of diffusion coefficient with respect to the number of data points. These errors were calculated from simulated images of particles exhibiting Brownian motion. Simulations of this experimental error reveal a decreasing trend with the number of data points. It will be shown (Appendix) that the error in the calculation of diffusion coefficient, resulting from pixelation, is bound by

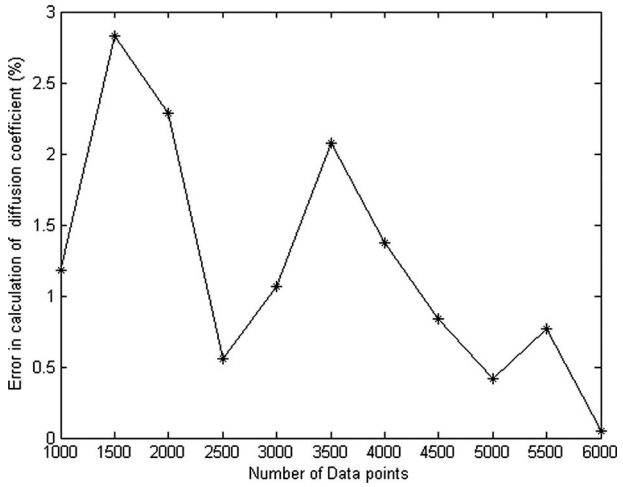

Fig. 6 Experimental error in the calculation of diffusion coefficient versus number of data points. These errors were calculated from simulated images of particles exhibiting Brownian motion.

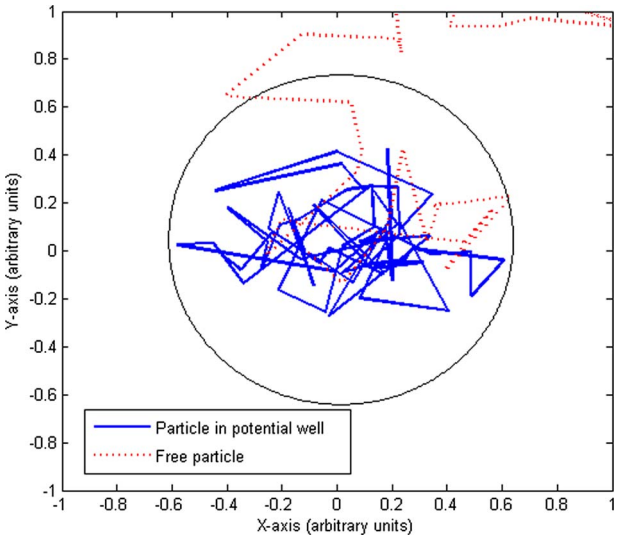

Fig. 8 Simulation runs of particles with and without a trap. The particle in a potential well exhibits a modified Brownian motion.

$$\text{Error} \leq O\left(\frac{\delta}{\sqrt{t}}\right) \tag{7}$$

where δ is an upper bound for the error in locating the particle centers. Eq. (7) reveals that this error can be reduced by making long time measurements.

Microparticles were successfully trapped in the optical trap, which appears in Fig. 7 as a bright spot approximately in the middle of the image. That the optical traps were effective in trapping the particles was confirmed by artificially inducing a flow and observing the movement of the trapped beads. The images provide positional data of the trapped beads. The higher the laser power used, the higher the trap strength and the lesser the observable Brownian motion.

Simulation runs (Fig. 8) show that the particle in an optical trap still exhibits a random walk behavior, which, however, is modified due to the presence of the potential well. Figure 9 shows the typical response of a particle in a trap. This response was captured using a frame rate of 155 frames/s.

Discussion

Advantages of Optical Diffusometry. The results show that binding of an analyte to an antibody functionalized particle can produce a significant decrease in its diffusion coefficient. Although the experiment used 0.69 μm particles, the method applies to particles as small as 40 nm [34]. Smaller particles undergo enhanced alteration in the diffusion coefficient, enabling detection of even smaller analytes.

The proposed technique offers four distinct advantages over affinity biosensors, which typically use sandwich assays for detection and measurement. Optical diffusometry uses a single antibody, which significantly reduces the reagent cost and enables virus detection with limited epitopes. Another advantage is the use of a label free detection mechanism. Sandwich assays usually involve an enzyme used as a signal reporter, which is limited by the availability of the detection conjugate. The proposed technique uses fluorescent particles, which serve the dual role of capturing and detecting. This combination simplifies the detection procedure. Thirdly optical diffusometry is much faster than sandwich assay. Typically this requires 30 min for virus binding and 15 min for optical detection and analysis. The assay can be finished within 1 h, whereas typical sandwich assays take 3–5 h [35]. Lastly, optical diffusometry can be multiplexed to detect multiple pathogens simultaneously. In order to multiplex the assay, par-

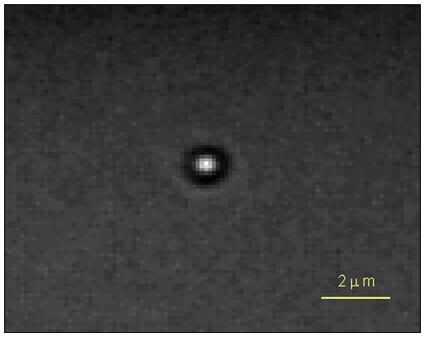

Fig. 7 A 0.69 μm particle (center) in an optical trap

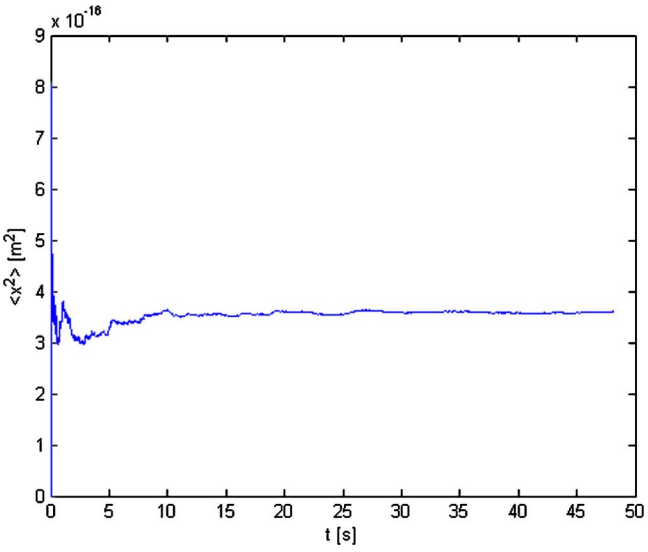

Fig. 9 Typical response of a bead confined to a small spatial volume by an optical trap

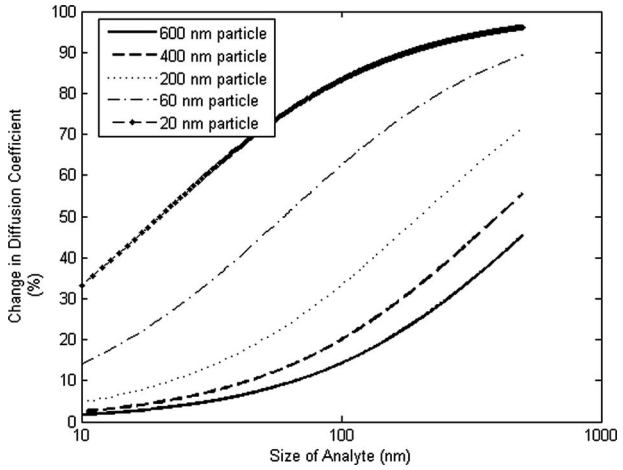

Fig. 10 Percentage change in the diffusion coefficient of virus-tagged beads as a function of the hydrodynamic radius of the pathogen

ticles with different colors can be coated with antibodies against different pathogens, and a mixture of particles can be used to detect multiple pathogens in a single assay.

Particle Tracking and μ-PIV. The particle tracking methodology applied here relies on a strong contrast between the background and the particle image. Fluorescent imaging usually provides such high contrast, but other methods like phase contrast microscopy may also be applied. μ-PIV, however, does not have such requirements [36]. In an optical trap since only a single particle is investigated, particle tracking is a natural choice. A particle in an optical trap is confined to a small spatial dimension. Hence one can use subpixel imaging, which enables the user to use a higher frame rate. A small dimension of 104×100 pixels only was imaged (Fig. 7), enabling the use of a higher frame rate of 155 frames/s.

Both Eqs. (3) and (4) are statistical in nature. For particle tracking Gaussian curve fitting can usually achieve good subpixel accuracy [7]. However, as will be shown in the Appendix, for particle tracking the calculation of D becomes more and more accurate by using longer time measurements irrelevant of the error in locating particle centers. This is confirmed by simulation results, as shown in Fig. 6. Error analysis for Eq. (4) is straightforward, and the peak width can typically be calculated with subpixel accuracy [37].

Sensitivity Analysis. The selection of bead diameter should be such that binding of the analyte has an appreciable change in its diffusion coefficient. We use for sensitivity analysis the same first order model that was used for correlation analysis. Assuming that the analytes can be characterized by a hydrodynamic radius, we get

$$\Delta D\,\% = \frac{r_{\text{virus}}}{r_{\text{virus}} + r_{\text{particle}}} \times 100 \tag{8}$$

The percentage change in diffusion coefficient is inversely proportional to the size of the particles used. Compared to a large particle, a smaller particle will undergo a more significant change in diffusion for a similar sized pathogen and hence can be used to detect smaller analytes. Figure 10 characterizes the change in diffusion coefficient as a function of this hydrodynamic radius. The model is simplistic in that it assumes that a virus can be characterized by a unique hydrodynamic radius, but it can give a good first guess. It should also be noted that the effective hydrodynamic radius of the virus need not coincide with its physical size. For viruses like the M13 phage virus, one way of calculating the corresponding hydrodynamic radius would be to correlate the increase in hydrodynamic drag (Eq. (5)) to the change in radius required to cause the variation (Eq. (8)). For example at a virus to bead ratio of 6:1, the calculated increase in hydrodynamic radius is 186 nm with a corresponding uncertainty of $\sim 5\%$.

Influence of Environmental Variables on the Resolution of Optical Diffusometry. Measurement of diffusion coefficient can be influenced by the variations of numerous factors, such as temperature, viscosity, and particle size. If the changes in these parameters are small, then a simple calculation shows that the influence of these changes can be expressed as

$$\frac{\delta D}{D} = \left(1 - \frac{T}{\mu}\frac{\partial \mu}{\partial T}\right)\frac{\delta T}{T} - \frac{\delta \mu}{\mu} - \frac{\delta r}{r} \tag{9}$$

Note that in the above equation it is assumed that the viscosity depends on temperature $(\partial \mu / \partial T)$ and on other factors as well $(\delta \mu)$. Variations in temperature can occur in each experiment due to radiation and absorption from the illumination source. A change of 0.1 K in absolute temperature changes the diffusion coefficient of particles by approximately 0.2%. Hence in controlled environments, temperature has a limited influence on diffusometry. Viscosity might independently change due to the presence of free viruses. The presence of particles in a medium changes the viscosity by [1]

$$\mu = \mu(1 + 2.5\phi) \tag{10}$$

where ϕ is the volume fraction of particles and viruses. Since in our case $\phi \ll 1$, the effect of particles on viscosity is small. The volume fraction of viruses is even smaller. Thus it appears that the variation in viscosity due to the presence of analytes and microparticles is quite small. By using multicolor beads of the same size, one can subject modified and unmodified particles to similar experimental conditions, thus minimizing errors due to such changes. Variations in microparticle size are unavoidable when using a population of particles.

Optical Trapping as a Multiplexing Tool and Its Role in Biosensing. Both the methods, particle tracking and μ-PIV, rely heavily on the necessity to extract a large number of images. It can be shown that the diffusion of trapped particles is quantitatively different from that of a freely diffusing particle. The diffusive behavior in the presence of such harmonic forces has been studied in detail. The statistics of such a particle becomes stationary in the long time, and it was established in Ref. [38] that

$$\lim_{t \to \infty} \langle \Delta x^2 \rangle = \frac{kT}{m\omega^2} \tag{11}$$

where ω is the angular frequency associated with the optical trap.

Equation (6) implies that the diffusion coefficient for a particle is zero irrespective of the strength of the trap or the variation in other parameters. Thus diffusive differential cannot be established by a study of the long time behavior. One alternative would be to establish a potential well with a "flat bed" and "steep walls." The walls would prevent the particle from escaping a given spatial domain, thus forming a cage. However, this requires the use of holographic optical traps, which has not yet been pursued in this work.

Another alternative is to study the diffusive behavior in the ballistic regime [39]. Although the long term behavior of a particle is independent of the particle drag, response on smaller time scales can also provide an insight. Figure 11 demonstrates the behavior of a particle in a trap, where two distinct regimes (linear and axiomatic convergences) are clearly depicted. The linear region can be used for the diffusion and drag differential study. In these small time scales, it is shown [39] that

$$\langle \Delta x^2(t) \rangle \approx 2Dt \tag{12}$$

Hence particle tracking can be done to establish drag differential between virus-tagged polystyrene beads. As can be seen in Fig. 9,

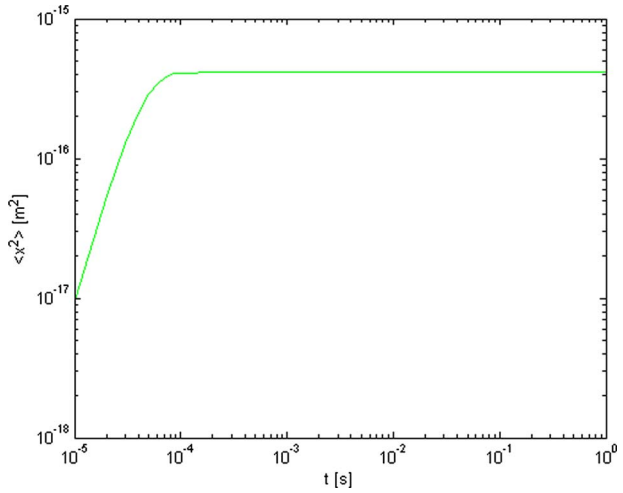

Fig. 11 A particle in a trap exhibits a linear trend on small time scales. This linear trend can be used for diffusion based differentiation. Note the extremely small time scales involved.

the response of the bead at low data acquisition rates does not reveal any information about the drag. For pathogen detection, high-speed cameras or other techniques, such as quadrant photodiode position detection, appear to be necessary.

Conclusion

This research demonstrates that binding of viruses on antibody functionalized particles results in a significant decrease in diffusion coefficients, which can be measured by particle tracking algorithms or μ-PIV techniques. Analytes, as small as 1 nm, can be detected by measuring the change in diffusion of antibody functionalized 40 nm particles. This method offers several advantages such as high spatial resolution, multianalyte detection capability, avoidance of sandwich assays, less preparation time, and quicker results. It is a more direct approach to biosensing compared to many other contemporary methods. The diffusion coefficient is measured from a population of particles. It was demonstrated that the experimental error due to pixelation depends not only on positional accuracy but also on the total data points used. This error decreases to zero with longer time measurements. This technology will be more powerful if accurate diffusion coefficients of single particles are measured. Optical traps offer such a technique, which is useful, even when the particles exhibit a modified Brownian motion. Optical traps make it feasible to locally constrain the particle in question for long time intervals, which then allows for extraction of a large amount of data. Static optical traps suffer from the shortcoming of having to require small time scale measurement techniques.

Appendix: Estimate of Error Due to Pixelation

According to the procedure outlined in the previous section, images of particles are acquired to yield the particle trajectories, which in turn are used to estimate the diffusion coefficient of particles. However, the trajectories suffer from discretization due to pixelation. The following analysis provides an estimate of this error.

Let $X(t)$ denote the n-dimensional Brownian motion process (where n can range from 1 to 3). Its probability density function (pdf) is given by $e^{-|x|^2/4Dt}/(4\pi Dt)^{n/2}$. The diffusion coefficient D and the mean square displacement is related by

$$D = \frac{\langle |X(t)|^2 \rangle}{2nt} \tag{A1}$$

where $\langle \cdot \rangle$ denotes statistical averaging.

Now let δ be half the pixel size. The measured diffusion coefficient denoted by D_δ is calculated as

$$D_\delta = \frac{\langle |X_\delta(t)|^2 \rangle}{2nt} \tag{A2}$$

where $X_\delta(t)$ is the experimentally obtained positional data. Note that $|X(t) - X_\delta(t)| \leq \delta$. The error in estimating the diffusion coefficient is thus

$$\begin{aligned} |D - D_\delta| &\leq \frac{1}{2nt} \int ||x|^2 - |x_\delta|^2| \frac{e^{-|x|^2/4Dt}}{(4\pi Dt)^{n/2}} d^n x \\ &\leq \frac{1}{2nt} \int ||x|^2 - |x \pm \delta|^2| \frac{e^{-|x|^2/4Dt}}{(4\pi Dt)^{n/2}} d^n x \\ &\leq \frac{1}{2nt} \int |2\delta|x| + \delta^2| \frac{e^{-|x|^2/4Dt}}{(4\pi Dt)^{n/2}} d^n x \\ &\leq O\left(\frac{\delta}{\sqrt{t}}\right) + O\left(\frac{\delta^2}{t}\right) \leq O\left(\frac{\delta}{\sqrt{t}}\right) \end{aligned} \tag{A3}$$

which indicates that the error goes to zero as $t \to \infty$. It should be noted that only the error due to pixelation is taken into account here.

References

[1] Einstein, A., 1956, *Investigations on the Theory of the Brownian Movement*, Dover, New York, p. 119.
[2] Langevin, P., 1908, "The Theory of Brownian Movement," C. R. Hebd. Seances Acad. Sci., **146**, pp. 530–533.
[3] Smoluchowski, M., 1906, "Zur Kinetischen Theorie der Brownschen Molekularbewegung und der Suspension," Ann. Phys.(Leipzig), **326**, pp. 756–780.
[4] Nelson, E., 1967, *Dynamical Theories of Brownian Motion*, Princeton University Press, Princeton, NJ, p. 142.
[5] White, F. M., 2006, *Viscous Fluid Flow*, McGraw-Hill Series in Mechanical Engineering, 3rd ed., McGraw-Hill, New York, p. 629.
[6] Crocker, J. C., 1997, "Measurement of the Hydrodynamic Corrections to the Brownian Motion of Two Colloidal Spheres," J. Chem. Phys., **106**(7), pp. 2837–2840.
[7] Crocker, J. C., and Grier, D. G., 1996, "Methods of Digital Video Microscopy for Colloidal Studies," J. Colloid Interface Sci., **179**(1), pp. 298–310.
[8] Park, J. S., Choi, C. K., and Kihm, K. D., 2005, "Temperature Measurement for a Nanoparticle Suspension by Detecting the Brownian Motion Using Optical Serial Sectioning Microscopy (OSSM)," Meas. Sci. Technol., **16**(7), pp. 1418–1429.
[9] Salmon, R., Robbins, C., and Forinash, K., 2002, "Brownian Motion Using Video Capture," Eur. J. Phys., **23**(3), pp. 249–253.
[10] Nakroshis, P., Amoroso, M., Legere, J., and Smith, C., 2003, "Measuring Boltzmann's Constant Using Video Microscopy of Brownian Motion," Am. J. Phys., **71**(6), pp. 568–573.
[11] Anderson, G. P., King, K. D., Gaffney, K. L., and Johnson, L. H., 2000, "Multi-Analyte Interrogation Using the Fiber Optic Biosensor," Biosens. Bioelectron., **14**(10–11), pp. 771–777.
[12] Eu, J. Y., Wang, C. Y., and Andrade, J., 1999, "Homogeneous Bioluminescence Assay for Galactosuria: Interference and Kinetic Analysis," Anal. Biochem., **271**(2), pp. 168–176.
[13] Liedberg, B., Nylander, C., and Lundstrom, I., 1983, "Surface-Plasmon Resonance for Gas-Detection and Biosensing," Sens. Actuators, **4**(2), pp. 299–304.
[14] Kharitonov, A. B., Wasserman, J., Katz, E., and Willner, I., 2001, "The Use of Impedance Spectroscopy for the Characterization of Protein-Modified ISFET Devices: Application of the Method for the Analysis of Biorecognition Processes," J. Phys. Chem. B, **105**(19), pp. 4205–4213.
[15] Saum, A. G. E., Cumming, R. H., and Rowell, F. J., 1998, "Use of Substrate Coated Electrodes and AC Impedance Spectroscopy for the Detection of Enzyme Activity," Biosens. Bioelectron., **13**(5), pp. 511–518.
[16] Cui, Y., Wei, Q. Q., Park, H. K., and Lieber, C. M., 2001, "Nanowire Nanosensors for Highly Sensitive and Selective Detection of Biological and Chemical Species," Science, **293**(5533), pp. 1289–1292.
[17] Saxton, M. J., 1997, "Single-Particle Tracking: The Distribution of Diffusion Coefficients," Biophys. J., **72**(4), pp. 1744–1753.
[18] Blair, D., and Dufresne, E., "The Matlab Particle Tracking Code Repository," http://physics.georgetown.edu/matlab/
[19] Santiago, J. G., Wereley, S. T., Meinhart, C. D., Beebe, D. J., and Adrian, R. J., 1998, "A Particle Image Velocimetry System for Microfluidics," Exp. Fluids, **25**(4), pp. 316–319.
[20] Olsen, M. G., and Adrian, R. J., 2000, "Brownian Motion and Correlation in Particle Image Velocimetry," Opt. Laser Technol., **32**(7–8), pp. 621–627.
[21] Hohreiter, V., Wereley, S. T., Olsen, M. G., and Chung, J. N., 2002, "Cross-Correlation Analysis for Temperature Measurement," Meas. Sci. Technol.,

13(7), pp. 1072–1078.
[22] Ashkin, A., Dziedzic, J. M., Bjorkholm, J. E., and Chu, S., 1986, "Observation of a Single-Beam Gradient Force Optical Trap for Dielectric Particles," Opt. Lett., **11**(5), pp. 288–290.
[23] Felgner, H., Frank, R., and Schliwa, M., 1996, "Flexural Rigidity of Microtubules Measured With the Use of Optical Tweezers," J. Cell. Sci., **109**, pp. 509–516.
[24] Kurachi, M., Hoshi, M., and Tashiro, H., 1995, "Buckling of a Single Microtubule by Optical Trapping Forces: Direct Measurement of Microtubule Rigidity," Cell Motil. Cytoskeleton, **30**(3), pp. 221–228.
[25] Henon, S., Lenormand, G., Richert, A., and Gallet, F., 1999, "A New Determination of the Shear Modulus of the Human Erythrocyte Membrane Using Optical Tweezers," Biophys. J., **76**(2), pp. 1145–1151.
[26] Suzuki, K., Sterba, R. E., and Sheetz, M. P., 2000, "Outer Membrane Monolayer Domains From Two-Dimensional Surface Scanning Resistance Measurements," Biophys. J., **79**(1), pp. 448–459.
[27] Ashkin, A., 1997, "Optical Trapping and Manipulation of Neutral Particles Using Lasers," Proc. Natl. Acad. Sci. U.S.A., **94**(10), pp. 4853–4860.
[28] Smith, S. P., Bhalotra, S. R., Brody, A. L., Brown, B. L., Boyda, E. K., and Prentiss, M., 1999, "Inexpensive Optical Tweezers for Undergraduate Laboratories," Am. J. Phys., **67**(1), pp. 26–35.
[29] Bechhoefer, J., and Wilson, S., 2002, "Faster, Cheaper, Safer Optical Tweezers for the Undergraduate Laboratory," Am. J. Phys., **70**(4), pp. 393–400.
[30] Buosciolo, A., Pesce, G., and Sasso, A., 2004, "New Calibration Method for Position Detector for Simultaneous Measurements of Force Constants and Local Viscosity in Optical Tweezers," Opt. Commun., **230**(4–6), pp. 357–368.
[31] Malagnino, N., Pesce, G., Sasso, A., and Arimondo, E., 2002, "Measurements of Trapping Efficiency and Stiffness in Optical Tweezers," Opt. Commun., **214**(1–6), pp. 15–24.
[32] Fields, B. N., Knipe, D. M., and Howley, P. M., 2007, *Fields' Virology*, 5th ed., Lippincott Williams and Wilkins, Philadelphia.
[33] Lee, G. U., Metzger, S., Natesan, M., Yanavich, C., and Dufrene, Y. F., 2000, "Implementation of Force Differentiation in the Immunoassay," Anal. Biochem., **287**(2), pp. 261–271.
[34] Csaki, A., Kaplanek, P., Moller, R., and Fritzsche, W., 2003, "The Optical Detection of Individual DNA-Conjugated Gold Nanoparticle Labels After Metal Enhancement," Nanotechnology, **14**(12), pp. 1262–1268.
[35] Crowther, J. R., 1995, *ELISA: Theory and Practice*, Humana, Totowa, NJ, p. 223.
[36] Hagsater, S. M., Westergaard, C. H., Bruus, H., and Kutter, J. P., 2008, "Investigations on LED Illumination for Micro-PIV Including a Novel Front-Lit Configuration," Exp. Fluids, **44**, pp. 211–219.
[37] Chamarthy, P., 2007, "Non-Intrusive Temperature Measurement Using Microscale Visualization Techniques," Ph.D. thesis Purdue University, West Lafayette.
[38] Chandrasekhar, S., 1943, "Stochastic Problems in Physics and Astronomy," Rev. Mod. Phys., **15**(1), pp. 1–89.
[39] Lukic, B., Jeney, S., Tischer, C., Kulik, A. J., Forro, L., and Florin, E. L., 2005, "Direct Observation of Nondiffusive Motion of a Brownian Particle," Phys. Rev. Lett., **95**(16), p. 160601.